Energy 163 (2018) 1062–1076

Contents lists available at ScienceDirect

Energy

journal homepage: www.elsevier.com/locate/energy

An appraisal of proportional integral control strategies for small scale waste heat to power conversion units based on Organic Rankine Cycles

Matteo Marchionni, Giuseppe Bianchi*, Apostolos Karvountzis-Kontakiotis, Apostolos Pesyridis, Savvas A. Tassou

Brunel University London, Institute of Energy Futures, Uxbridge, Middlesex, UB8 3PH, UK

ARTICLE INFO

Article history:
Received 9 April 2018
Received in revised form
30 July 2018
Accepted 20 August 2018
Available online 22 August 2018

Keywords:
Waste heat recovery
Organic Rankine cycle
Radial turbo-expander
Plate heat exchanger
Dynamic modelling
PI control strategy

ABSTRACT

Despite the increasing number of Organic Rankine Cycle (ORC) installations at megawatt scale, the waste heat rejected by industrial processes can vary substantially from a few kWh to many megawatt hours. Hence, ORC units with a power output in the range of tens of kilowatts should be developed to tackle the heat recovery and business opportunities that can arise from this market segment. In the current research activity, a dynamic model of a small scale ORC system was developed using a commercial software platform. The unit is equipped with two plate heat exchangers, a centrifugal pump and a radial turbine designed and optimized using an in-house code and a commercial 1D modelling tool. The off-design behaviour of the ORC system has been characterized by varying the inlet conditions of heat source and sink, and the revolution speed of the turbomachines. Moreover, the response to transient thermal inputs at different time scales has also been investigated. Finally, four control strategies have been compared from the performance and energy efficiency perspectives. The results show that the turbine based regulation strategies achieve better control performance while pump based controls are able to regulate the system by maintaining the net power output closer to the design point.

1. Introduction

The growing energy demand, the scarcity of fossil sources, and the increasing stringent regulations on the pollutants and the greenhouse gas emissions are driving academia and industry to seek new solutions for a sustainable power generation and to increase the overall energy efficiency of existing industrial facilities. Among the Waste Heat Recovery (WHR) technologies, heat to power conversion systems represent one of the most effective methods to reduce the industrial net energy consumption and enhance the re-use of the heat recovered in a flexible and profitable way. Usually these waste heat sources are available at low temperatures and are widespread in industry. For such cases, the Organic Rankine Cycle (ORC) technology has proven to be a reliable, cost-effective and easy to maintain technology [1–3], especially for large capacities ranging from a few hundreds of kW_{th} to a few MW_{th} [4–7].

When smaller units are considered in the power input range of a few kilowatts up to 100 kW_e, there are aspects which have not been fully investigated yet. Among them, one of the most relevant topics is the accurate modelling of the system dynamics for design and optimization purposes [8], and the development of suitable and effective control strategies, to ensure safe and optimal operation of the unit even when sudden changes in the operating conditions occur. The latter is strongly needed in several applications, as the automotive ones or distributed stand-alone units, where flexibility and reliability in different working points are fundamental. In such applications, the heat load supplied to the system can change rapidly in a periodic, random and unexpected way, as it occurs for example in automotive ORC systems under transient driving cycles [9]. For these reasons, the proper modelling and analysis of transients, together with the design of suitable control systems is crucial and requires further attention.

In Ref. [10] Desideri et al. developed a model of a 11 kW_e ORC system equipped with a screw expander. The model was validated in steady-state and transient conditions by imposing step change in the pump revolution speed of 5 Hz and 15 Hz. The results showed a

* Corresponding author.
E-mail address: giuseppe.bianchi@brunel.ac.uk (G. Bianchi).

https://doi.org/10.1016/j.energy.2018.08.156

good accuracy in predicting the system transients even if difficulties were found to handle the zero-flow conditions occurring when shut down and start-up operations are considered. An even smaller system has been analyzed by Kosmadakis at al. in Ref. [11], who studied a supercritical 3 kW ORC engine equipped with a volumetric scroll expander. The system was tested in on design and off-design conditions and the effect of the turbomachines' revolution speed on the unit performance was assessed. Another low capacity ORC system using a volumetric expander as power conversion unit was modelled by Quoilin et al. in Ref. [12]. The aim of the work was to test three different control strategies able to optimize the system overall efficiency when the hot source inlet temperature was varied from 120 °C up to 300 °C. The control variables adopted were the pump and the expander revolution speeds. It has been found that the regulation of the evaporating temperature of the working fluid, accomplished by setting the revolution speed of the volumetric expander, achieved the best performance. Similar control strategies have been developed by Ni et al. in Ref. [13] for a larger ORC system recovering heat through a solar parabolic collector. Even in this case only the transient dynamics of the heat exchangers were reproduced, while steady state models were used for the turbomachines. A model for a much higher capacity ORC system was proposed by Mazzi et al. [14]. The ORC unit was designed to recover heat from a stream of exhaust gases of 58.9 kg/s at 300 °C. The authors were able to reproduce the behaviour of the system at off-design and transients conditions. The results showed that the performance of the unit was affected by the change of the inlet temperature of the heat source. A decrease in the oil temperature of 30 °C resulted in a system efficiency drop from 24.6% to 23.6%.

Similar work was carried out by Casella and Mathijssen [15] on a 150 kW_e ORC system using a turbo-generator as power conversion device. The model was successfully validated, showing an uncertainty of nearly 3% between the experimental measurements and model predictions. The authors also designed a Proportional-Integral (PI) controller to regulate the turbine inlet temperature acting on the pump revolution speed. The feed-back controller showed good performance but more complex regulation systems may be required to handle a wider range of operating conditions. A Proportional-Integral-Derivative (PID) scheme coupled with a feed-forward and a lead-lag compensator was implemented and compared to more conventional PID controllers by Usman et al. [16]. The results showed that the controller was able to track the expander speed and cope well with electric load disturbances. Another work on the control of the turbine generator of an ORC system was carried out by Padula et al. [17], focused in particular on the switching of the unit from the grid operating mode to stand-alone mode through a series of throttle valves placed at the inlet of the high and low temperature/pressure turbines. Usman et al. [16] also presented strategies oriented at controlling the power output of a small scale off-grid ORC unit equipped with a scroll expander [16].

More advanced control strategies have been proposed by Hernandez et al. [18,19]. The authors compared the model predictive and extremum-seeking control techniques against the more conventional PID regulations. They reported that more advanced strategies, thanks to a more efficient control action, allow an increase of the energy recovery compared to PID schemes. However, when the objective is to manage reduced time scale disturbances introduced by temperature and flow fluctuations of the waste heat source rather than optimize the power output of the ORC unit for different heat load conditions, the added complexity of these control methods may represent an obstacle to their widespread use in industrial WHR applications, which demand simple and cost-effective solutions.

For these reasons, the aim of this work was to investigate several control strategies, each one characterized by different complexity, to assess their performance and suitability for small scale ORC systems for stationary WHR applications. The novelty of the study involved the testing of the control strategies on a fully dynamic ORC model, considering the transient behaviour of all the components of the system, including turbomachines, valves and system piping. The model refers to a 40 kW ORC power unit equipped with a radial turbine whose design has been accomplished by means of a novel approach additionally reported in the paper. After the description of the modelling methodology, the off-design behaviour of the ORC unit is presented and the transient responses of both the uncontrolled and controlled system are assessed with reference to a series of heat load profiles at different time scales (200s, 350s, 600s and 1100s). Four different control strategies are also implemented and compared. All the strategies adopt a Proportional-Integral (PI) control law to maintain constant the Turbine Inlet Temperature (TIT) for different control parameters.

2. Dynamic model

The research methodology herein presented is applicable to any ORC based heat to power conversion unit. The transient and control studies performed, instead, mostly refer to stationary power generation systems. In particular, the applications where the conclusions presented in this study can be transposed are the ones where water is either the waste heat stream (e.g. geothermal ones) or the heat transfer fluid from a heat recovery exchanger. With regards to the second case however, the current modelling approach discards the thermal inertia of the heat recovery loop, which in turn can damp high frequency fluctuations of the heat load at the ORC evaporator.

With reference to the plant scheme in Fig. 1, the heat recovery takes place through a plate heat exchanger having water on the hot side and the working fluid of the system, which is R245fa, on the cold side. After being pressurized in a multi-stage centrifugal pump, the working fluid undergoes to a full vaporization during the heat recovery process and it is expanded in a turbine, where the useful energy conversion process takes place from a slightly superheated state. After the expansion, the working fluid is eventually condensed in a second plate heat exchanger using water as heat sink. A refrigerant receiver is eventually positioned between the condenser and the pump such that thermal expansion during start-up or large transients can be absorbed, and any cavitation phenomenon at the pump inlet is prevented.

The commercial software platform in which the modelling has been carried out is GT-SUITE™. This tool includes model templates for the components employed in the plant configuration considered. Nevertheless, accurate input data are of paramount relevance for the overall implementation and accuracy of the approach. These inputs can result either from an experimental campaign or, as in the current case, from more detailed or complex models. Finally, connections between these devices are made through piping sub-models. The electric machines connected to pump and turbine are not modelled in this work, which means that the power quantities considered are purely mechanical. In the following paragraphs, a more detailed description of each sub-model is provided.

The boundary conditions imposed in the simulations are revolution speeds of pump and turbine as well as inlet temperatures and flow rates of hot and cold sources. The equations are solved with an implicit numerical method that approximates the system of algebraic differential equations to a system of nonlinear algebraic ones, which are eventually solved iteratively. The solution values at the next time step are simultaneously provided to all the sub-volumes of a given model (e.g. pipes divisions, heat exchangers

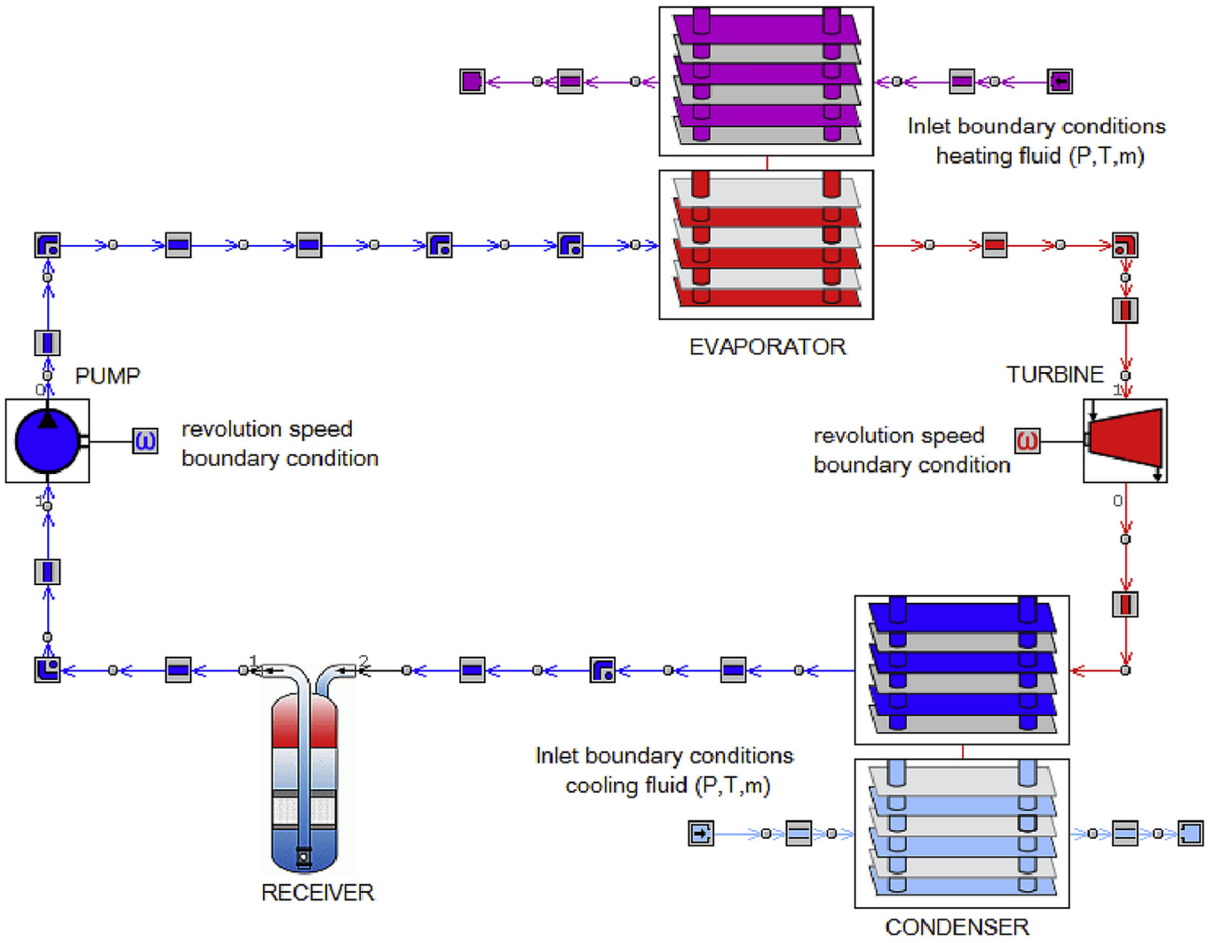

Fig. 1. GT-SUITE™ scheme of the ORC model [20].

channels etc.) [21] and the thermodynamic properties of the working fluid are interfaced with the solver through a dynamic-link library of the NIST Refprop database [22].

2.1. Evaporator and condenser

To model the evaporator and the condenser, a simulation tool provided by a well-known OEM has been used to retrieve several operating points of the two plate heat exchangers manufactured by the same company [23]. These operating points have been obtained by varying several model inputs, such as the refrigerant mass flow rate; the inlet temperature of the refrigerant; and the inlet and outlet temperatures of the cold and hot sources. The output data were instead the temperatures and the quality of the refrigerant at the outlet of the heat exchangers; the cold and hot source mass flow rates; and the pressure losses on both sides. These quantities have been eventually entered into the plate heat exchanger template of GT-SUITE™ to calculate the best fitting coefficients of Nusselt-Reynolds (Nu-Re) correlations eventually used to compute the heat transfer coefficients along the equivalent one-dimensional passages with whom the heat exchanger channels are approximated [24]. In particular, these input data are used to fit the best Nu-Re curve specifically for the non-refrigerant side, while for the refrigerant one, well-known correlations are adopted to predict the heat transfer [21].

The heat exchanger channels, whose geometry is specified by the user, are discretized in a finite number of sub volumes following the staggered grid approach. This method consists in assuming the scalar thermodynamic quantities (as pressure, density, temperature, etc.) as constant and equal to the ones considered in the centroid of each sub volume, and calculating instead the vector quantities (as the mass or the flow velocity) at their boundaries [21]. The vector quantities plus the pressure and the total enthalpy of the fluid are computed by solving the one dimensional continuity, momentum and enthalpy equations (Eqs. (1)–(3)). The other scalar quantities not specified at the beginning of the process are instead calculated through the fluid property library.

$$\frac{dm}{dt} = \sum_{bound} \dot{m} \tag{1}$$

$$\frac{d(\rho H_0 \mathrm{v})}{dt} = \sum_{bound} (\dot{m} H_0) + \mathrm{v}\frac{dp}{dt} - hA\left(T_{wf} - T_{wl}\right) \tag{2}$$

$$\frac{d(\dot{m})}{dt} = \frac{dpA + \sum_{bound} (\dot{m}\mathrm{v}) - 4\zeta\frac{\rho \mathrm{v}|\mathrm{v}|}{2}\frac{dxA}{D} - \xi\left(\frac{\rho \mathrm{v}|\mathrm{v}|}{2}\right)A}{dx} \tag{3}$$

To predict the phase change, the formation of vapour bubbles or liquid droplets is addressed by evaluating the fluid density in each sub volume, while the extension of the two-phase area is computed following the vapour Rayleigh-Plesset formulation [25], reported in Eq. (4).

$$\frac{p_b - p_\infty}{\rho} = R\frac{d^2R}{dt^2} + \frac{3}{2}\left(\frac{dR}{dt}\right)^2 + \frac{4v}{R} + \frac{2\sigma}{\rho R} \quad (4)$$

Therefore, based on these predictions, the software applies different correlations according to the fluid phase. In particular, the Dittus-Boelter correlation is used in single phase heat transfer (Eq. (5) if the fluid is being heated or Eq. (6) if the fluid is being cooled) [24], while in the two-phase region, the correlation from Yao et al. (Eq. (7)) has been considered for the condenser [26] and the one from Donowsky and Kandlikar (Eq. (8)) for the evaporator.

$$h = 0.023\ \mathrm{Re}^{0.8}\ \mathrm{Pr}^{0.4}\frac{k}{D} \quad (5)$$

$$h = 0.023\mathrm{Re}^{0.8}\mathrm{Pr}^{0.3}\frac{k}{D} \quad (6)$$

$$h = 4.118\mathrm{Re}_{eq}^{0.4}\mathrm{Pr}_l^{1/3}\frac{k_l}{D} \quad (7)$$

$$h = \left(1.1837Co^{-0.3} + 225.5Bo^{0.7}\right)(1-x)^{0.003}h_l \quad (8)$$

In these correlations, the terms Co, Bo and Re_{eq} in Eqs. (7) and (8) are respectively the convection, the boiling and the equivalent Reynolds numbers, and they can be calculated according to Equations (9)–(11). The term h_l in Eq. (8) represents the heat transfer coefficient calculated through the Dittus-Boelter correlations and considering the properties of the liquid as inputs.

$$Co = \left(\frac{1-x}{x}\right)^{0.8}\left(\frac{\rho_v}{\rho_l}\right)^{0.5} \quad (9)$$

$$Bo = \frac{q''}{\dot{m}(h_v - h_l)} \quad (10)$$

$$\mathrm{Re}_{eq} = \frac{m''(1 - x + x\sqrt{\rho_l/\rho_v})D}{\mu_l} \quad (11)$$

The thermal inertia due to the heat exchanger material is also discretized along the flow path. In particular, depending on the discretization length (20 sub-volumes per pass) a series of metallic blocks is generated knowing the geometrical features of the heat exchanger (dimensions, number of passes, presence of fins, etc.) and the temperature dependency of the physical properties of the material (stainless steel 304) such as thermal conductivity, specific heat and density. All this information are input parameters of the model and are reported in Table 1 where slave refers to the cold fluid of the heat exchanger, i.e. R245fa for the evaporator and water for the condenser.

The model block diagram representative of the first two channels of the discretized plate heat exchanger is eventually reported in Fig. 2. The series of blue and red blocks relate to the discretized cold and hot channels respectively, which are connected to the metallic plates of the heat exchanger by means of thermal convective connections (grey circles). The series of blocks representing the discretized dry masses of the plates (squared blocks with a dot in the middle) are connected together by thermal conductive connections.

Table 1
Summary of the heat exchangers specifics.

Geometrical dimensions	Evaporator	Condenser
Plate length [mm]	694.00	
Plate width [mm]	304.00	
Plate dry mass [kg]	0.68	
Plate material	304 L stainless steel	
Channel height [mm]	2.29	
No. of channels (R245fa side)	99	129
No. of channels (Water side)	100	130

2.2. Pump

The pump has been modelled by calculating its performance and isentropic efficiency maps by means of a 2D interpolation based on a set of operating points available on the website of the manufacturer, and expressed in terms of pressure rise, volumetric flow rate and power consumption. Regarding the performance map (Fig. 3), since the real data were available only for a limited range of revolution speeds, namely between 1800 and 3000 RPM, the performance curves for speeds lower than 1800 RPM have been computed using a linear extrapolation method. The isentropic efficiency map instead (Fig. 4), has been calculated based on the interpolated power consumption data.

2.3. Piping and receiver

Straight pipes have been considered as one dimensional ducts with a circular cross section and with a roughness value typical for stainless steel. Additional bends have been modelled using the software library that already contains the localized pressure drops

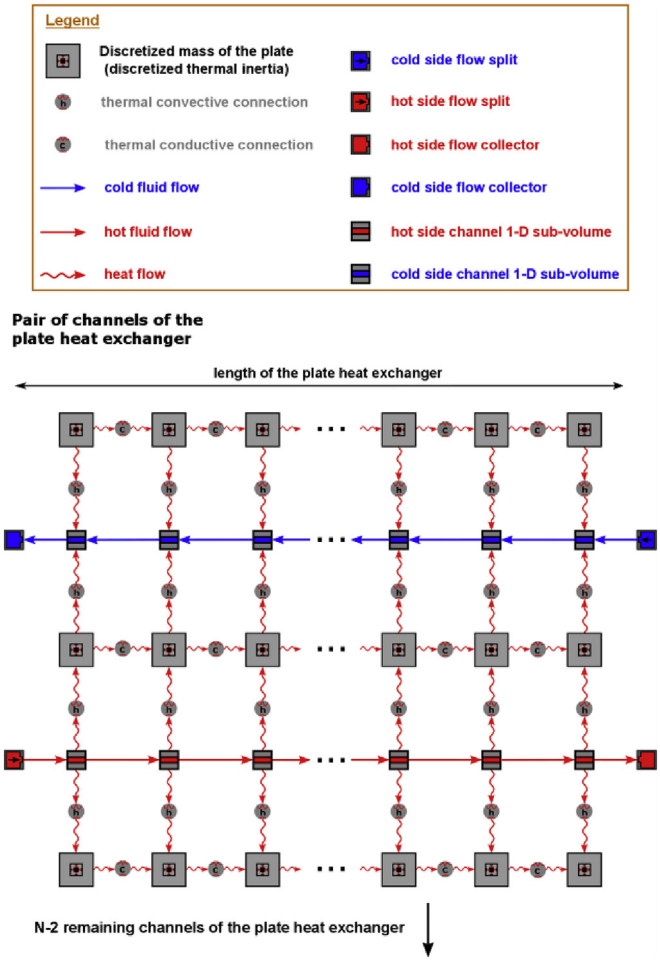

Fig. 2. Detailed model block diagram for plate heat exchangers [21].

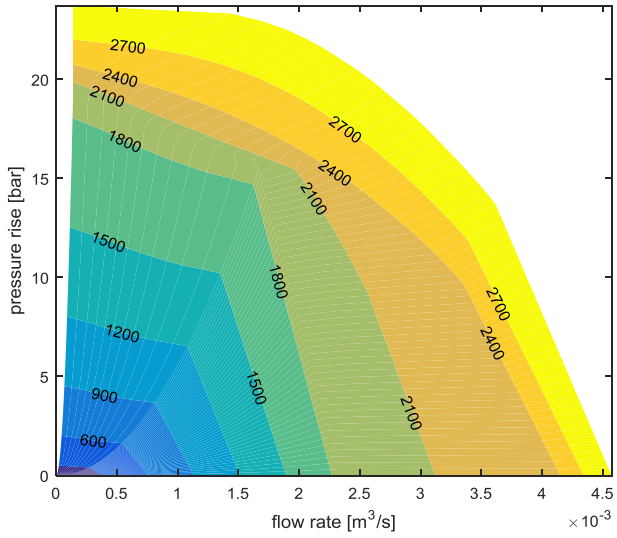

Fig. 3. Pump performance map (contour lines in RPM).

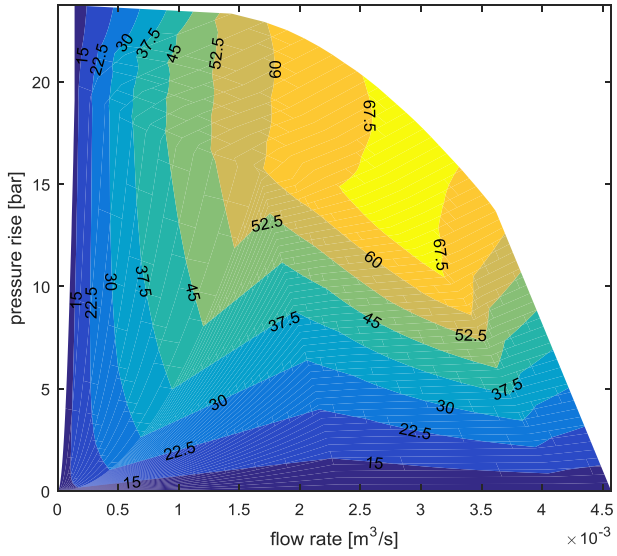

Fig. 4. Pump efficiency map (contour lines in percentage).

due to such components. For sake of simplicity, assuming that the pipes are insulated, adiabatic conditions were set to prevent any heat loss to the environment. The receiver size was chosen to be 0.02 m^3, i.e. the 25% of the system capacity [21].

3. Radial turbine model

The mean-line modelling of the radial inflow turbine consists of three main steps: the design process, the optimization process and finally the off-design analysis. The design and optimization methods are based on an in-house code which is described in details below and further presented in Ref. [27]. The design process is utilized to calculate the main geometric characteristics of the expander. Through the optimization one based on Sequential Quadratic Programming (SQP), the obtained turbine geometry is modified according to a user defined objective function and aerodynamic or manufacturing constraints. The final turbine geometry is therefore imported in the off-design analysis to calculate the expander performance at various pressure ratios, mass flow rates, and revolution speeds.

3.1. Design method

The design method applies a mean-line approach to design the three main components of the turbine namely volute, stator and rotor. Fig. 5 schematically illustrates the expansion process using the Mollier diagram across the stage. Initially, the working fluid is peripherally accelerated via the volute (1–2) and undergoes to a further increase of its circumferential velocity via the stator (2–3). Therefore the fluid is isentropically mixed in the intermediate space between stator and rotor (3–4) before its kinetic energy is converted in mechanical one (4–5). The basic equations of the real and isentropic enthalpy drops, as well as the turbine power output are described in Equations (12)–(15). Finally the turbine design model calculates the main geometrical quantities of the turbine as per the parameters in Fig. 6.

$$\Delta H_{is} = H_{01} - H_{5s} \tag{12}$$

$$\Delta H_{real} = \eta_{ts} \Delta H_{is} \tag{13}$$

$$\dot{W}_o = \dot{m} \Delta H_{real} \tag{14}$$

$$w_o = u_4 v_{\theta 4} - u_5 v_{\theta 5} \tag{15}$$

The mean-line model uses an iterative method to calculate the thermodynamic properties and the turbine geometry at the station points of the three main components of the expander. The method also employs the loss mechanisms to more accurately estimate the turbine total to static isentropic efficiency. The calculation flowchart is schematically presented in Fig. 7, where the sub models of the rotor, stator, volute and loss correlations are employed. Convergence is achieved when the difference between the assumed and calculated total to static isentropic efficiency (η_{ts}) is less than the convergence error.

The modelling of the rotor geometry and the calculation of the velocity triangles of the radial rotor are thoroughly outlined in Ref. [28]. Loading and flow coefficients are user defined non-dimensional parameters and stand for the real enthalpy drop and the volumetric flow rate of the rotor respectively.

$$\psi = \frac{\Delta H_{real}}{u_4^2} \tag{16}$$

$$\varphi = \frac{v_{m5}}{u_4} \tag{17}$$

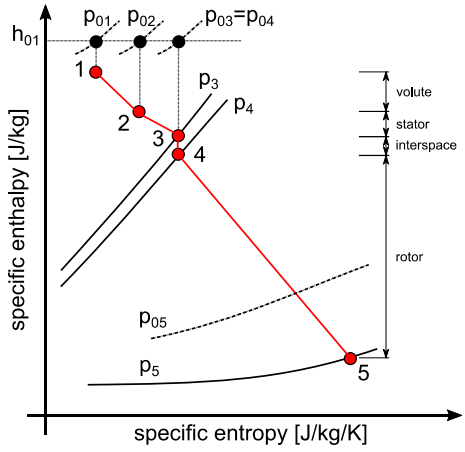

Fig. 5. Mollier diagram of the full turbine stage.

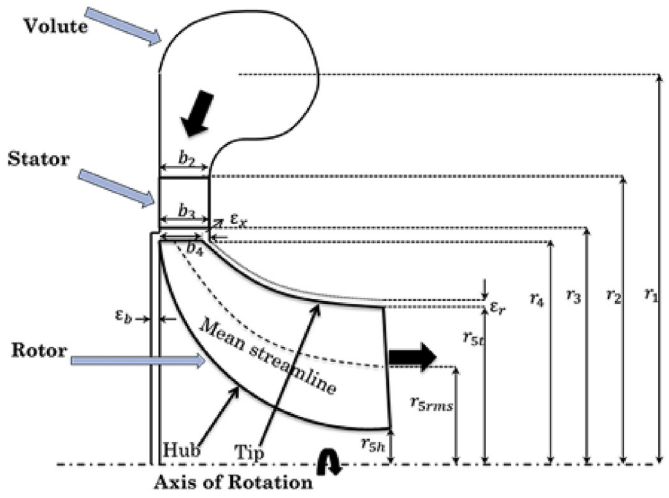

Fig. 6. Turbine stage geometry.

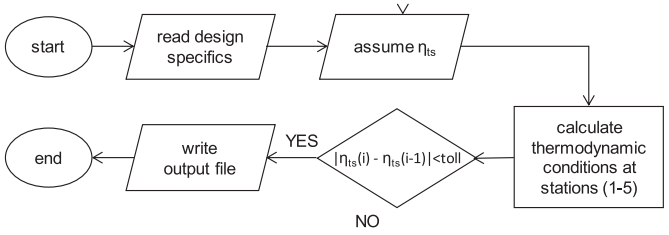

Fig. 7. Turbine design algorithm.

The loading (ψ) and flow (φ) coefficients are optimized using the SQP optimization algorithm and the user defined constraints. Then, the peripheral speed u_4 and the meridional velocity c_{m5} at the rotor outlet can be calculated and the velocity triangles at its leading edge are finally computed (Fig. 5). Under design conditions, $c_{\theta 5}$ should be minimum; therefore in this work it was assumed equal to zero. The velocity triangle at the rotor exit can be calculated using appropriated trigonometry rules. Stagnation and static thermodynamic properties are calculated from Refprop at each station. Finally, the isentropic efficiency is defined as follows:

$$\eta_{ts} = \frac{H_{01} - H_{05}}{H_{01} - H_{5s}} \tag{18}$$

The main functionality of the stator is to guide and accelerate the flow velocity and to remove any circumferential non-uniformity. In this work, stator simulation is based on the method proposed by Aungier [29]. The design procedure of the nozzle vanes are performed iteratively and a blade thickness distribution on a parabolic arc camber-line is imposed. The imposition of the geometry allows to calculate the thermodynamic properties and flow angles using the mass and energy balance equations.

Volute modelling includes the calculation of the primary volute passage area. The latter is performed by calculating the mean radius using the mass conservation and the angular momentum equations. The optimum radius value is computed from the optimization method, which calculates the turbine diameter which corresponds to the maximum isentropic efficiency. The loss model in this study is expressed in terms of enthalpy drop and reported below for each component of the turbine. A first assumption of the total-to-static efficiency is required in order to proceed with the preliminary design of the turbine stage. Then, the new value of the efficiency is calculated after considering turbine losses reported in Equations (19)–(22). Blade angles are measured with respect to the axis of rotation. Table 2 summarizes inputs, geometry and performance of the radial turbo-expander at design point.

$$\Delta H_{inc} = \frac{1}{2}\left[W_4 \sin\left(\beta_4 - \beta_{4,opt}\right)\right] \tag{19}$$

$$\Delta H_{pass} = \frac{1}{2}\left(2\zeta \frac{L_{hyd}}{D_{hyd}}\overline{W}^2 + \frac{R_4 c_4^2}{R_c Z_r}\right) \tag{20}$$

$$\Delta H_{tip} = \frac{u_4^3 Z_r}{8\pi}\overline{w}^2 \left(K_x \varepsilon_x v_x + K_r \varepsilon_r v_r + K_{x,r}\sqrt{\varepsilon_x \varepsilon_r v_x v_r}\right) \tag{21}$$

$$\Delta H_o = \frac{1}{2}c_5^2 \tag{22}$$

3.2. Off-design analysis

After this design stage, the commercial 0D/1D commercial software Rital® has been used to calculate the turbine performance and isentropic efficiency maps, which accurately describe the expander behaviour under off-design conditions. Firstly Rital® was calibrated in order to predict the expander design point. Then it was used to calculate the off-design performance of the turbine. Last but not least, these operating maps obtained with the aforementioned approach have been implemented in GT-SUITE™ and are reported in Figs. 8 and 9.

4. Results and discussion

The design of the ORC system and its component was performed aiming at a power output of 40 kW from a water stream of 10 kg/s at 110 °C. However, since the scope of the current research goes beyond the design phase, the results of the design process are just recalled and summarized in Table 3. The results that are going to be

Table 2
Summary of turbo-expander design with reference to dimensions shown in Fig. 6.

inputs	T_1	101	°C
	p_1	11.6	bar
	p ratio	3.6	–
	$\dot{m}$	2.86	kg/s
volute	r_1	119.0	mm
stator	r_2	98.5	mm
	b_2	3.0	mm
	r_3	75.8	mm
	b_3	3.0	mm
rotor	r_4	72.4	mm
	b_4	3.0	mm
	r_{5t}	35.1	mm
	r_{5h}	14.5	mm
	b_5	20.6	mm
	α_3	57.2	°
	β_4,blade	−25.0	°
	α_4	56.3.0	°
	β_4	−45.0	°
performance	power	40	kW
	η_{ts}	57.1	%
	φ	0.4	–
	Ψ	0.6	–
	Z_{rot}	8	–
	Z_{st}	11	–

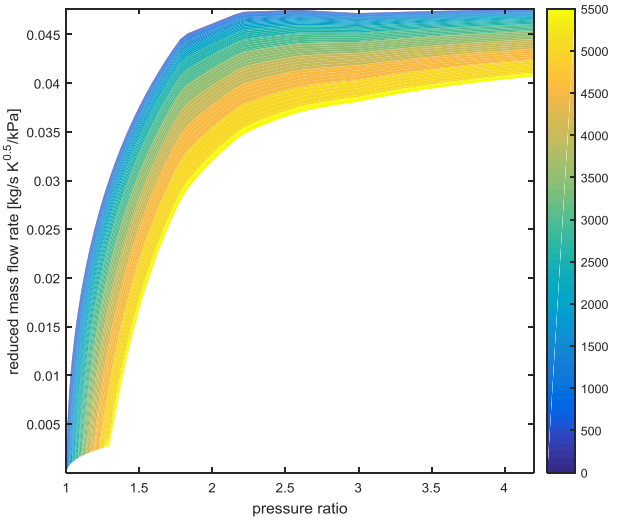

Fig. 8. Non dimensional turbine performance map ($T_{01} = 375$ K, color bar in reduced RPM). (For interpretation of the references to color in this figure legend, the reader is referred to the Web version of this article.)

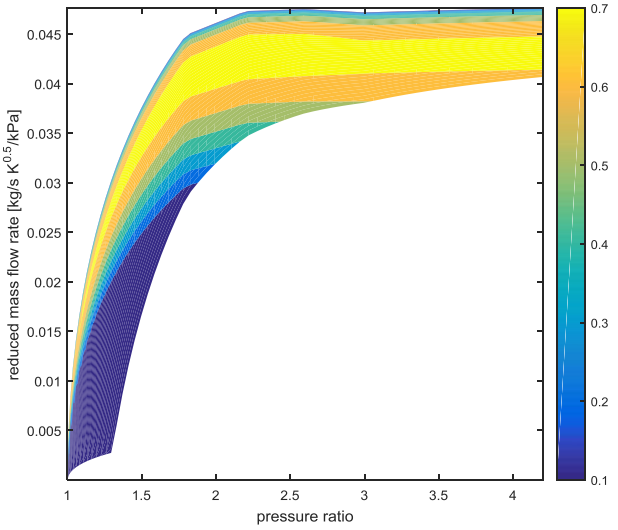

Fig. 9. Turbine total-static efficiency map ($T_{01} = 375$ K).

presented include a first set of simulations to understand the off-design and dynamic features of the unit. Based on this information, the last analysis concerns with the implementation and verification of different PI control strategies.

4.1. Off-design performance

The steady state performance of a given ORC system mainly depends on the inlet conditions of the hot and the cold sources, and on the revolution speeds of pump and expander. The system behaviour at off-design conditions has been therefore assessed through three sets of simulations in which one of these parameters at a time was modified with respect to the design point. Moreover, in these analyses no control measure was established.

In the first series of simulations, the heat recovery has been varied acting on both mass flow rate and temperature of the heat source at the evaporator inlet. Their relative effects on the ORC system performance have been analyzed and reported in Figs. 10 and 11. In particular, Fig. 10 shows the net power output and the

Table 3
Operating conditions of the ORC power unit at the design point.

Refrigerant: R245fa	Model I/O	Design	
Mass flow rate	Output	2.86	kg/s
Evaporating pressure	Output	11.6	bar
Evaporating temperature	Output	96	°C
Turbine inlet temperature	Output	101	°C
Condensing pressure	Output	3.2	Bar
Condensing temperature	Output	48	°C
Hot source: Water			
Mass flow rate	Input	10	kg/s
Inlet temperature	Input	110	°C
Inlet pressure	Input	3.0	Bar
Cold source: Water			
Mass flow rate	Input	14.31	kg/s
Inlet temperature	Input	35	°C
Inlet pressure	Input	1.0	bar
Pump			
Revolution speed	Input (Range 600–3000)	2600	RPM
Isentropic efficiency	Output	70	%
Power	Output	7	kW
Turbine			
Revolution speed	Input (Range 6000–60000)	30000	RPM
Isentropic efficiency	Output	57.1	%
Power	Output	40	kW
ORC unit			
Net power output	Output	40	kW
Overall efficiency	Output	5	%

thermal efficiency of the ORC unit varying the hot source mass flow rate and maintaining the hot source inlet temperature constant and equal to the design value. Conversely, Fig. 11 reports the results of the same analysis but varying the hot source inlet temperature and maintaining constant its mass flow rate. From the comparison between the two analyses, it is possible to notice that the hot source inlet temperature affects the net power output of the unit more predominantly than the hot source mass flow rate. Indeed, when

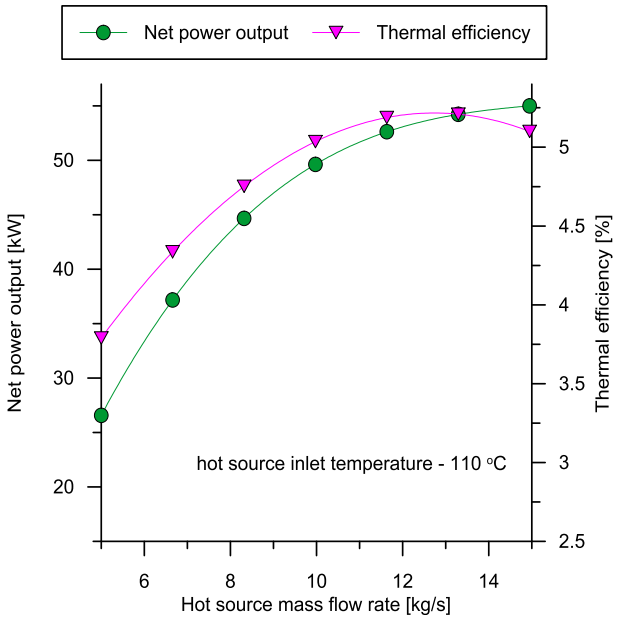

Fig. 10. System performance varying the hot source mass flow rate (constant inlet temperature).

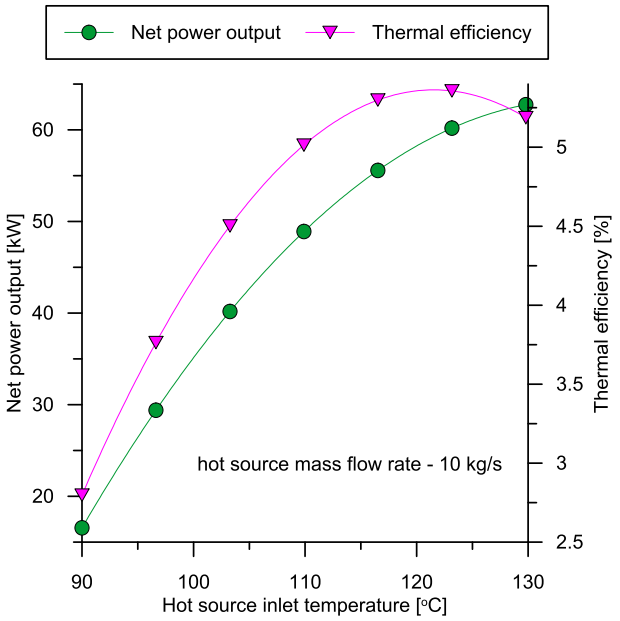

Fig. 11. System performance varying the hot source inlet temperature (constant mass flow rate).

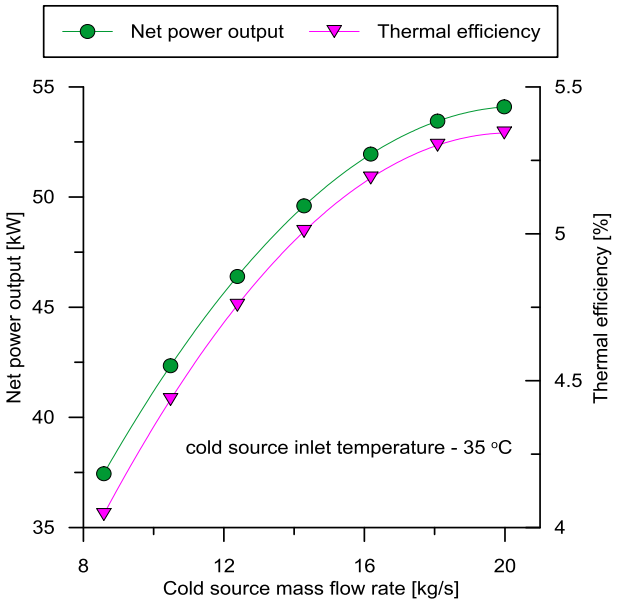

Fig. 12. System performance varying the cold source mass flow rate (constant inlet temperature).

the mass flow rate of the hot source is changed between 8 kg/s and 12 kg/s, the net power output generated glides from 43 kW to 52 kW, which corresponds to the 86.0% and the 102.0% respectively of the nominal power (Fig. 10). For the same relative change in the hot source inlet temperature (i.e. from 90 °C to 130 °C) the power output of the system goes from 28 kW up to 57 kW, the 58.0% and the 114.0% respectively of the nominal value (Fig. 11). Similar considerations apply for the overall efficiency. Such a higher sensitivity can be explained by analyzing the behaviour of the evaporator at off-design conditions. In fact, when a variation of the hot source temperature at the inlet of the heat exchanger occurs, it directly affects, besides the fluid superheating, the evaporating pressure of the working fluid and thus the net specific work of the system. Instead, a variation of the hot source mass flow rate from the design point, mainly affects the working fluid superheating, which in turn has less influence on the power generated. Therefore, operating the evaporator at lower loads leads to a flow of superheated refrigerant with a slightly lower pressure ratio across the turbine, which in turn extracts less power. When the heat exchanger is instead overloaded, the increase of power is again due to a slightly augmented refrigerant mass flow rate and evaporating pressure, which occurs to accommodate the new pinch point in the evaporator due to the increased heat load. Moreover, the saturation of the device can be noticed from Fig. 10, which shows that a constant increasing hot source mass flow rate of 11 kg/s, 13 kg/s and 15 kg/s leads to a gradually decreasing increment of net power output of 52 kW, 54 kW and 55 kW respectively.

Similarly, Figs. 12 and 13 show the ORC unit performance as a function of the heat sink inlet conditions, being the other operating parameters kept at the design values. In particular, Fig. 12 relates the net power output and the thermal efficiency of the system as a function of the cold source mass flow rate, while Fig. 13 refers to the cold source inlet temperature variation. In both cases positive effects can be achieved on the system performance. When in fact the mass flow rate of the heat sink is increased to 20 kg/s, which is an increase of 40.0% respect to the design condition, the net power output and the thermal efficiency of the unit go up to 54 kW and 5.3% respectively, which correspond to the 106.0% of their

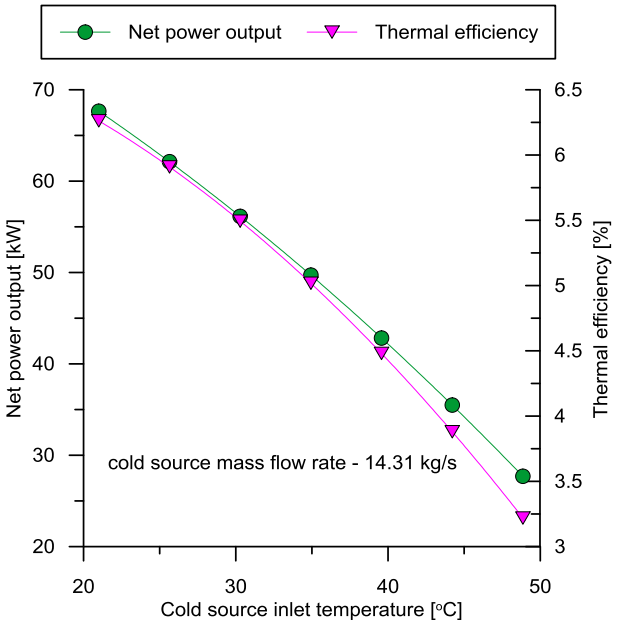

Fig. 13. System performance varying the cold source inlet temperature (constant mass flow rate).

respective nominal values. Even more beneficial effects are given from an inlet temperature decrease of the heat sink, which allows the ORC unit to achieve a net power output and a thermal efficiency of 68 kW and 6.3% respectively when the cooling water inlet temperature is decreased to 21 °C. The performance rise is due to the decrease of the condensing pressure of the working fluid and a consequent decrease of the refrigerant temperature at the inlet of the pump. Indeed, while the first effect leads to an augmented expansion ratio across the turbine; the second one allows to reduce the pumping power since the density of the refrigerant at the inlet of the device is increased.

Finally, the effects of the variation of the pump and the turbine

revolution speed on the ORC performance have been investigated and shown as maps in Figs. 14 and 15. In particular, Fig. 14 shows the overall ORC efficiency as a function of the pump and the turbine revolution speeds, while Fig. 15 highlights the net power output. From both figures the design point of the system can be easily identified. Furthermore, both figures report that the islands of maximum efficiency and net power output (highlighted in yellow) are much more extended in the pump revolution speed direction rather than in the expander one. In fact, regarding the thermal efficiency, an optimal value of 5.0% is achievable for a pump revolution speed that goes from 2600 RPM up to 3000 RPM, the 115.0% of the nominal value, while the optimal operating range for the turbine goes from 30000 RPM to 32000 RPM, which is only the 107.0% of the design value. This is of particular interest for control purposes, since it clearly shows that adopting the pump revolution speed as a manipulating variable, rather than the turbine one, can ensure a wider control margin to achieve the twofold objective of regulating the system while still operating at optimal conditions.

4.2. Transient analysis

In the simplest architecture, such as the one investigated in the current study, an ORC system is at least composed of two heat exchangers and one receiver. These components are not only filled with large quantities of working fluid but also have metallic surfaces whose thicknesses allow to withstand high pressures. The thermal inertia due to these coexisting effects acts as a low pass filter for the ORC system and needs to be taken into account when developing a control system for an ORC unit, especially if the final application is a transportation one.

In order to stress and demonstrate this concept, transient simulations were carried out on the modelled ORC system. In particular, the simulations imposed a variable mass flow rate at the hot side of the evaporator and observed the effects on the turbine inlet temperature (TIT), a fundamental parameter of the ORC operation. Fig. 16 summarizes the transient analysis with respect to a steady state value marked with SS. The grey line refers to the input while the black one to the output. The mass flow rate profile is composed of two ramps and two plateaus. Durations of the transient inputs are 200, 350, 600 and 1100s. Both shape and duration of the transient inputs have been arbitrarily chosen with the purpose of providing a thorough yet still general analysis.

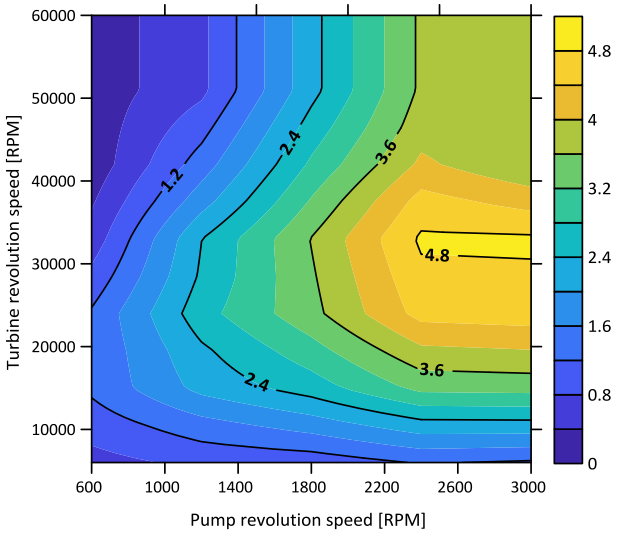

Fig. 14. ORC unit thermal efficiency as a function of the pump and the turbine revolution speeds.

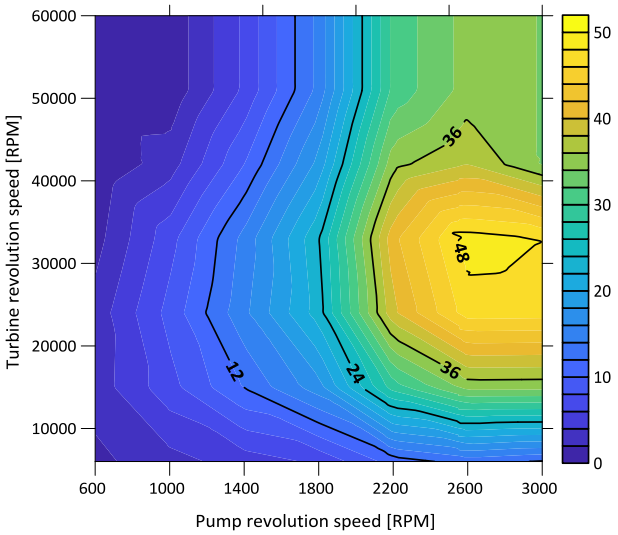

Fig. 15. ORC unit net power output as a function of the pump and the turbine revolution speeds.

The comparison between the different heat load profiles in Fig. 16 can give an idea about the magnitude of the thermal inertia of the system. For a quick heat load transient, Fig. 16 a shows that the response of the TIT presents a consistent delay, being able to achieve again the steady state value approximately 60s after hot stream mass flow disturbance occurs, and does not reproduce any intermediate plateau in its trace. When the transient input is slower (Fig. 16b), although the temperature overshooting after the first ramp is still delayed, about approximately 25s, the temperature trend starts to resemble the mass flow rate profile and resolve the intermediate plateaus. Negligible delays in the TIT response instead occur when the time scale of the heat load transient profile is increased (Fig. 16 c and d), in turn characterized by a confident reproduction of the mass flow rate input. In all the cases, the TIT shows a 10 °C increment or decrement with respect to the steady state value (approximately ±10%) following a 20% increase or decrease respectively from the design point of the hot source mass flow rate. Both this positive and negative variations of the turbine inlet temperature could be potentially dangerous for the ORC unit. In fact, an excessive superheating could compromise the chemical stability of the organic working fluid, while, inversely, a sudden decrease of the heat load could lead to a decrease of the quality of the working fluid and a consequent formation of liquid droplets downstream the evaporator, which can potentially damage the turbo-expander.

Therefore, it is crucial to develop suitable control strategies able to prevent or at least limit these harmful and undesired operating conditions. The results also suggest that different control strategies should be adopted for heat loads at different time scales. For instance, when the hot source presents slow variations in time, as in Fig. 16 c and d as well as typically in stationary applications, the time constants of the heat exchanger and the one of the variation are comparable. In turn, the temperature of the working fluid at the turbine inlet could be set acting on the mass flow rates of the evaporator, thus manipulating the pump revolution speed or using by-pass valves. Instead, when more rapid changes of the heat load are considered, as in Fig. 16a and . b an action on the mass flows can result trivial, and the regulation of a variable with a faster dynamics is required. In this sense, acting on the turbine speed might be a viable solution since this parameter affects the evaporating

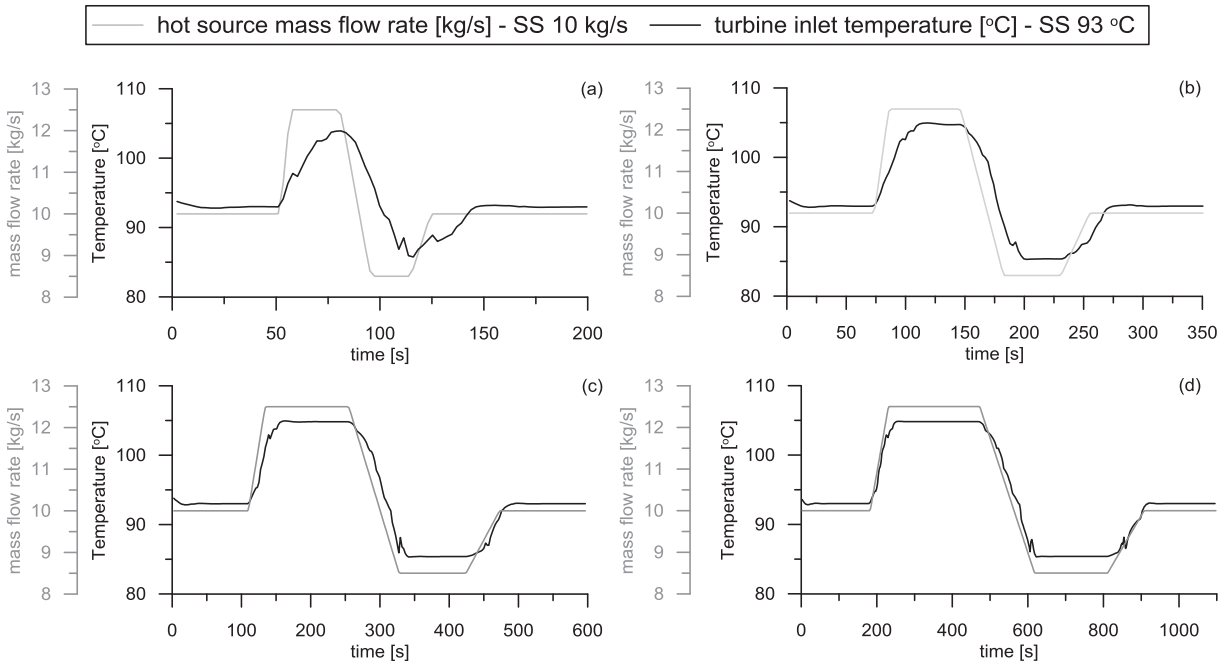

Fig. 16. Transient simulations (no control).

pressure inside the evaporator. In general however, as it will be shown in the next section, the thermal inertia of the system and the extreme interdependency between the system variables introduce delays in the control action, limiting its effectiveness and promptness.

4.3. Control strategies

The ORC system herein modelled is a stationary one. As shown in Fig. 15, it has been designed to get the maximum output power and overall efficiency at the nominal operating point reported in Table 3. Therefore, rather than large shifts in the operating conditions, only some deviations to the nominal heat input are expected. For these reasons, the control of ORC unit aimed at maintaining the maximum output power by keeping the turbine inlet temperature (TIT) to the target nominal value. As previously discussed, additional motivations to control the maximum cycle temperature are the chemical integrity of the working fluid and the functional safety of the turbo-expander.

To achieve this target, given the same transient heat load profiles shown in Fig. 16, four approaches have been tested, each of them characterized by a different set of manipulated variables: the pump revolution speed (OP = Only Pump strategy), the turbine revolution speed (OT = Only Turbine strategy), the pump and the turbine revolution speed (PT = Pump and Turbine strategy), and the pump revolution speed together with the opening position of a recirculating valve (PV = Pump and Valve strategy). In this last option, when the valve is fully open (for an angle of 90°), the nominal value of the refrigerant mass flow rate (2.86 kg/s) is laminated and diverted from the outlet of the pump directly to the inlet of the condenser, excluding therefore the evaporator and the expander (Fig. 17). The normal flow path is instead restored once the valve is fully closed. The various discharge coefficients versus the different opening angles of the valve have been supplied by a manufacturer and have been used to model the valve in GT-SUITE™. The use of this strategy allows also to eventually reduce the heat duty at the condenser (because of the merging of cold liquid and vapour flow at the inlet of the latter), which can be beneficial in various applications [9].

Regarding the control law, each strategy utilizes a Proportional-Integral (PI) controller to reduce the error between the actual turbine inlet temperature and the target one. The derivative term has been set to zero because of the high control action that can result in case of noisy signals. Furthermore, in order to prevent the saturation of the control action caused by the integral term, an anti-wind up scheme has been adopted. The tuned proportional and integral coefficients for each different strategy, whose gain have been adjusted via a calibration procedure, are reported in Table 4. The system is considered as a black box and the control calibrated by adjusting the gains following the response of the controlled variable to a step off the manipulated one, which varies depending on the strategy considered.

Even if this approach allows to reduce the implementation complexity of the control system, it does not allow to take into account the effect of the coupling between several main thermodynamic variables affecting the ORC power unit behaviour, therefore limiting the promptness and the effectiveness of the regulation. However, as it will be shown in the next section, the control strategies implemented show good performance, especially considering that they have been tested on a very detailed model, which takes in account all the thermal inertia effects introduced by the consistent fluid and metallic masses characterizing the ORC unit.

4.3.1. Simulation results using control strategies

The results related to the testing of the several control strategies implemented are shown in Fig. 18. In particular, the first line of figures (Fig. 18 a-.d) refers to the Only Pump (OP) strategy, the second line (Fig. 18 e-h) to the Only Turbine (OT) one; while the third (Fig. 18 i-l) and the fourth (Fig. 18 m-p) to the Pump and Turbine (PT) and to the Pump and Valve (PV) strategy respectively. In each case is possible to notice the effect of the thermal inertia of the ORC system on the control action, limiting its effectiveness and promptness.

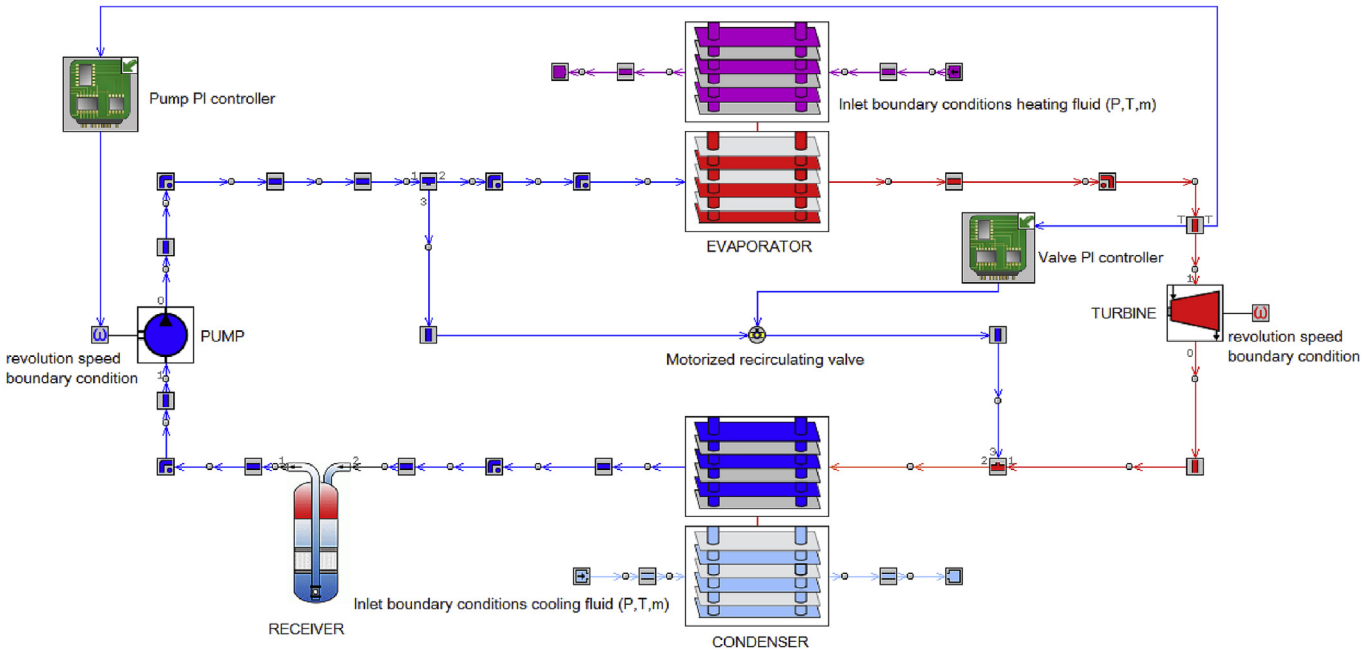

Fig. 17. Control implementation in the ORC model (Pump and Valve control strategy).

Table 4
PI controller coefficients for the different regulation strategies.

Controller coefficients	Proportional	Integral
Only Pump (OP)	−71	−0.33
Only Turbine (OT)	−4000	−27.78
Pump and Turbine (PT)	−40 (P); −4000 (T)	−0.12 (P); −27.78 (T)
Pump and Valve (PV)	−40(P); 1 (T)	−0.20(P); 0.02 (T)

In the OP case for instance, for quick transients (Fig. 18a and b), the controller is not able to reject the disturbance introduced by the hot source mass flow rate variation, and the controlled response of the system equals the uncontrolled one. When instead the heat load transient become slower, the regulation of the TIT is accomplished effectively. In particular, both Fig. 18 c and d show that the control system is able to limit the time at which the TIT achieves the highest percentage variation (±10%), preventing therefore the thermal degradation of the working fluid and ensuring safe operating conditions for the expander. In fact, in the first case (Fig. 18c) the intermediate plateaus are reduced from 150s (uncontrolled system) to approximately 40s (controlled system); while in the second one (Fig. 18d), from 250s (uncontrolled system) to nearly 50s (controlled system). For this slowest transient thermal load, which constraints the ORC unit to operate in off-design conditions for several minutes, the control system is able to lower the maximum TIT from 102 °C (uncontrolled system) to nearly 96 °C (controlled system) when the working fluid is overheated; and to raise the minimum TIT from 85 °C (uncontrolled system) over 93 °C (Fig. 18d), when the heat load is reduced. A further point of interest are the overshoots noticeable in both Fig. 18 c and 18. d, which are mainly due to the non-collocated action of the regulation. Indeed, the temperature sensor that provides the actual value of the TIT is located after the evaporator, while the actuation, exerted by the pump in this case, takes place before the heat exchanger. This results in a change of the relative position between the zeros and the poles of the closed loop system transfer function on the complex plane, whose are not anymore alternated as it occurs in collocated control systems; and in turn in a reduced stability and performance of the controller.

With respect to the pump revolution speed, the manipulation of only the turbine one (OT strategy) ensures a faster response of the controlled system. In fact, even if also in this case the most rapid disturbance is not rejected (Fig. 18e), when a higher time scale thermal load transient is considered (Fig. 18f), the controller is able to partially act on the controlled variable by increasing the evaporating pressure, and thus the TIT, from 85 °C (uncontrolled case) up to 88 °C (controlled case). However, the lower plateau is increased from 35s to 85s and the controller is not able to reduce the TIT when the hot source mass flow rate is increased (Fig. 18f). The control strategy is quite effective also for slower transient thermal inputs (Fig. 18g and h), setting the temperature at 98 °C and 88 °C when the hot source mass flow rate is increased and decreased respectively. Furthermore it is possible to notice that the overshoots occurring in the OP strategy are avoided, thanks to the collocation of the sensor and the actuation (both located after the evaporator). Instead, a reduced effectiveness is noticeable when the amount of hot source mass flow rate supplied to the evaporator is decreased for a prolonged time interval.

The effectiveness of the regulation in these cases can be improved by adopting as control variable the pump revolution speed in addition to the turbine one (PT control strategy). In fact, Fig. 18k and l shows the better performance achieved by such controller. In particular, when a 600s thermal input is considered (Fig. 18k), the controller is able to reduce the plateaus of the TIT and quickly reduce the error between its actual value and the target one. For a slower thermal input transient, the controller shows even higher performance, being able to reduce the TIT from 102 °C (uncontrolled case) to 94 °C (controlled case) when the hot source mass flow rate increases; and to rapidly reduce the settling time, with respect to the previous strategies analyzed, when the hot source mass flow rate is decreased (Fig. 18l). Furthermore, this particular choice of control variables allows to limit the overshoots in the controlled system response. However, for faster thermal transients input (Fig. 18 i and j), the regulated TIT is consistently delayed, since its intermediate plateaus are increased from 3s to 50s (Fig. 18i) and from 35s to 100s (Fig. 18) when the hot source

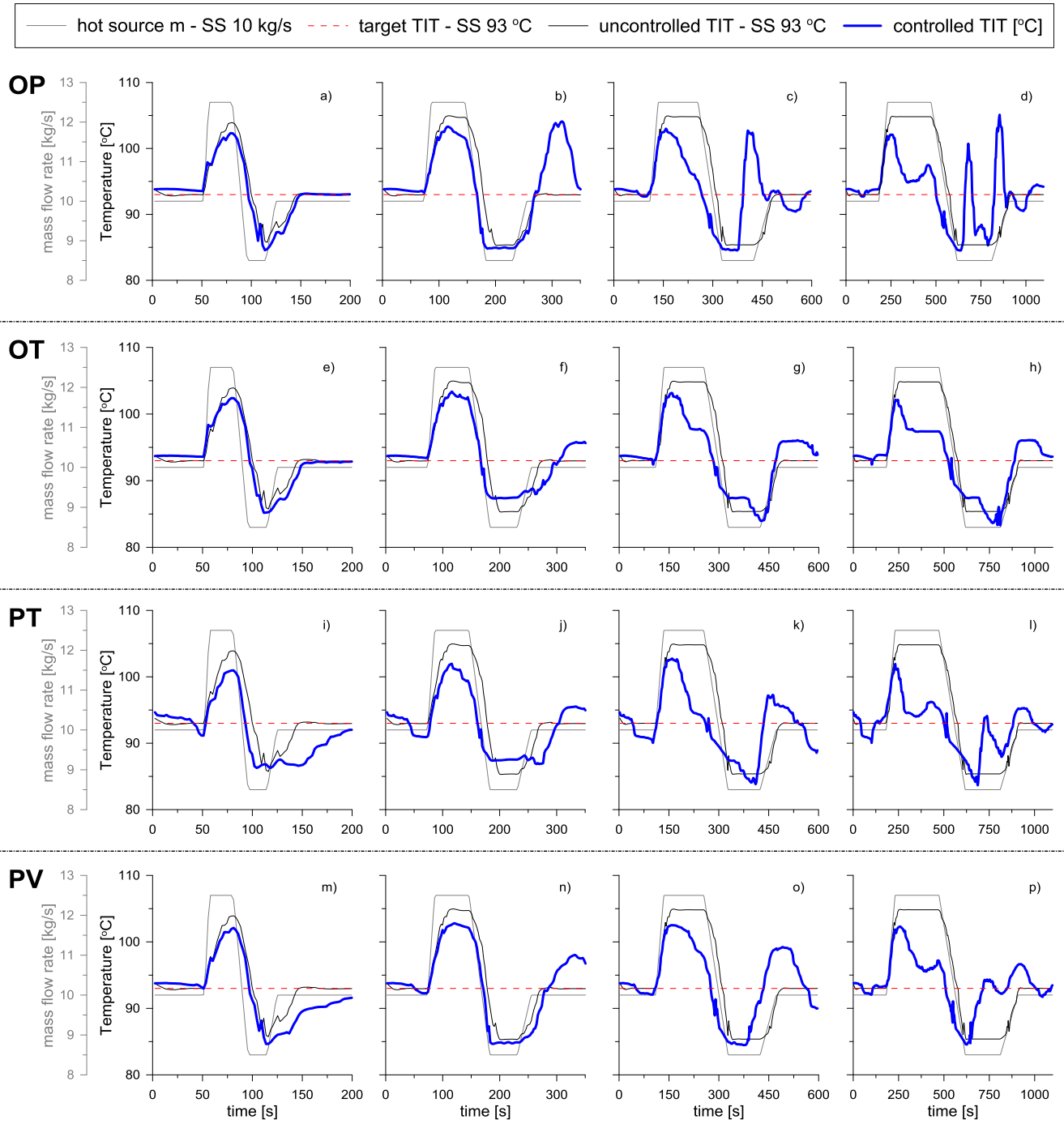

Fig. 18. Transient response of the ORC unit at different heat load variations with and without the control of the turbine inlet temperature.

mass flow rate is suddenly decreased to the 85% of its nominal value.

Finally, the results of the simulations related to the use of the Pump and Valve (PV) control strategy are reported. Also in this case the controller is not able to regulate effectively the TIT when the hot source mass flow rate rapidly varies with time (Fig. 18 m and 18. n). For slower transients instead, the strategy implemented results effective, being able to reduce the intermediate plateaus for which the TIT achieves its maximum and minimum variations from 150s (uncontrolled system) to nearly 60s (controlled system) (Fig. 18 o); and from 250s (uncontrolled system) to nearly 50s (controlled system) (Fig. 18 p). Furthermore, the addition of the recirculating valve to the system allows to reduce the overshoots, which characterize the system controlled response when only a pump regulation is implemented. This is mainly due to the faster response the recirculating valve guarantees. Bypassing in fact the evaporator, the valve is able to quickly reduce the mass flow rate of working fluid flowing into the heat exchanger and therefore the thermal inertia of the system. This translates also in a substantial reduction of the regulation settling time, noticeable in Fig. 18 p, when a lower amount of heat load is provided to the ORC unit. However, notwithstanding the good performance this strategy achieves, the use of a recirculating valve implies a lamination of the working fluid, which is always not preferable from an energy efficiency

perspective.

In conclusion, the results show that all the strategies are able to regulate the system and reject the heat load disturbances introduced by the waste heat source, especially when slower transient thermal loads are considered. The results are not profile dependent, since the gains of the control are not adjusted on a single transient thermal input. Therefore, similar performance of the control strategies are expected if different time varying heat load profiles are given as input to the system.

However, when fast transients are imposed, the controllers are not effective, in particular the ones based on the manipulation of the pump revolution speed. As already stated above, this is due mainly to the thermal inertia of the system, which in this work is fully taken in account by the developed model. On the other hand, the approach adopted does not allow a detailed analysis of the interactions between the different thermodynamic variables affecting the system behaviour; and consequently neither the development of more advanced control strategies which could overcome these issues and guarantee better performance of the regulation.

4.3.2. Control strategies comparison

The results of the comparison from an energy efficiency perspective of the four control strategies investigated in this manuscript are reported in Fig. 19. Among the approaches investigated, the one adopting the turbine revolution speed as the manipulated variable have proved to be the least efficient mainly because of the narrow optimal operating range of the expander. In fact, when a given transient thermal load with a time scale of 1100s is supplied to the evaporator, the ORC unit regulated by the OT and the PT strategies is able to produce an overall amount of energy equal to 11.6 kWh and 12.0 kWh respectively, which is lower than the 14.7 kWh and 15.2 kWh produced when the OP and PV regulations are used (Table 5). Fig. 19 shows in detail in fact, that during the hot source mass flow rate variations, the consequent manipulation of the turbine revolution speed outside the optimal design values leads to a drop in the expander isentropic efficiency and therefore in the ORC net power output.

Indeed, when the hot source mass flow rate is increased from 10 kg/s to 12 kg/s, the ORC power output is reduced from 50 kW to 40 kW, because the controller raises the turbine revolution speed to increment the working fluid mass flow rate and consequently balance the higher heat load provided to the evaporator. The power output of the unit is even further cut down, close to 10 kW (Fig. 19), when the hot source mass flow rate is decreased from 10 kg/s to 8 kg/s, because of the drastic expander revolution speed truncation to decrease the refrigerant mass flow rate flowing into the system. This explains the slightly higher efficiency of the PT strategy that compared to the OT one achieves in the same case a net power generation of nearly 30 kW, being able to count on the manipulation of the pump revolution speed to decrease the refrigerant mass flow rate.

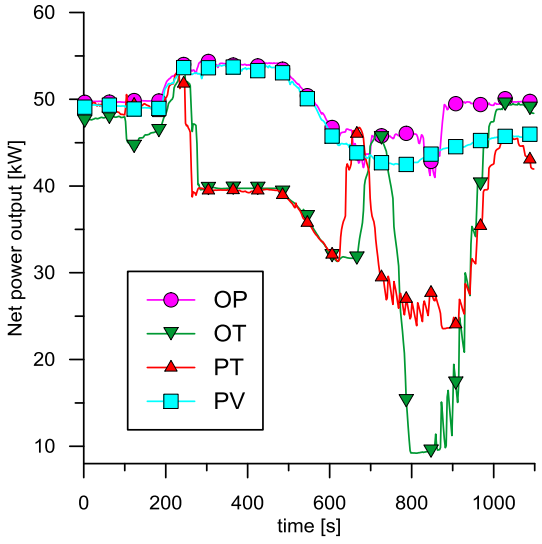

Fig. 19. Comparison of controlled power outputs for the 1100s transient heat load profile presented in Fig. 16 d.

Table 5
Energy recovered in Fig. 19.

Control strategy	Energy recovered [kWh]
Only Pump (OP)	15.2
Only Turbine (OT)	11.6
Pump and Turbine (PT)	12.0
Pump and Valve (PV)	14.7

The pump based regulation instead allow to have a flatter power generation profile when the same transient thermal input is applied to the system. In fact, when the ORC system is regulated using the OP and the PV control strategies, it is able to produce 55 kW when the heat load is increased and on average 47 kW and 43 kW respectively when the heat load is decreased (Fig. 19). The reason for that lies in the higher optimal operating range of the pump and mainly in the fact that the power required to pressurize the fluid does not affect considerably the ORC unit net power output. Furthermore, it is possible to notice from this analysis the negative effect from an energy efficiency perspective of adopting a recirculating valve to control the system, which can be accounted as nearly a 5 kW penalization on the ORC power outcome compared to an only pump based regulation (Fig. 19).

5. Conclusions

This paper reports on investigations of the dynamic response of a 40 kW Organic Rankine Cycle waste heat to power conversion unit to transient loads and on the performance of different control strategies for the system based on proportional-integral controllers. The research methodology involved a commercial software package and performance data for the system components which were obtained from more complex modelling approaches. In particular, the operating maps of the radial turbo-expander were generated from a novel mean line design and optimization methodology.

The off-design simulations highlighted the large impact the radial turbo-expander speed has on the overall energy recovery performance. The results also showed that the influence of the heat source and sink temperatures on system performance is greater than that of the mass flow rates of the heat source and heat sink fluids.

The response of the ORC unit to transient heat loads at different time scales (200, 350, 600 and 1100s) further emphasized the delay in the variation of the expander inlet temperature due to a change of the heat source mass flow rate, especially at fast time scales. This is due to the thermal inertia of the fluids and of the metallic parts of the plate heat exchangers.

The comparison of four PI control strategies showed that the turbine based strategies may achieve better thermodynamic system performance where the pump based strategies, for the same transient thermal input, are able to maintain the net electrical power output closer to the design point.

Acknowledgement

Aspects of the work have been funded by: i) the Centre for Sustainable Energy Use in Food Chains (CSEF) of Brunel University London. CSEF is an End Use Energy Demand Centre funded by the Research Council UK (RCUK), Grant No: EP/K011820/1; ii) Engineering and Physical Sciences Research Council (EPSRC) under project EP/P004636/1, Optimizing Energy Management in Industry 'OPTEMIN'. The authors would like to acknowledge the financial support from the EPSRC as well as contributions from Mr. Marek Lehocky and Mr. Jonathan Harrison of Gamma Technologies during the model development. The manuscript reports all the relevant data to support the understanding of the results. More detailed information and data, if required, can be obtained by contacting the corresponding author of the paper.

References

[1] Angelino G, Gaia M, Macchi E. Review of Italian activity in the field of organic rankine cycles. VDI Berichte. 1984. p. 465–82.
[2] Verneau A. Waste heat recovery by organic fluid rankine cycle. 1979.
[3] Carcasci C, Ferraro R, Miliotti E. Thermodynamic analysis of an organic Rankine cycle for waste heat recovery from gas turbines. Energy 2014;65:91–100. https://doi.org/10.1016/J.Energy.2013.11.080.
[4] Alle. One MW binary cycle turbogenerator module made in Europe. Proc World Geotherm Congr 1995;3:2125–30.
[5] Kaplan U. Advanced organic rankine cycles in binary geothermal power plants, vol. 8. Ormat Technol Inc; 2007. http://www.ormat.com/research/papers/papers3.
[6] Astolfi M, Romano MC, Bombarda P, Macchi E. Binary ORC (Organic Rankine Cycles) power plants for the exploitation of medium-low temperature geothermal sources - Part B: techno-economic optimization. Energy 2014;66:435–46. https://doi.org/10.1016/j.energy.2013.11.057.
[7] Franco A. Power production from a moderate temperature geothermal resource with regenerative Organic Rankine Cycles. Energy Sustain Dev 2011;15:411–9. https://doi.org/10.1016/j.esd.2011.06.002.
[8] Wei D, Lu X, Lu Z, Gu J. Dynamic modeling and simulation of an Organic Rankine Cycle (ORC) system for waste heat recovery. Appl Therm Eng 2008;28:1216–24. https://doi.org/10.1016/j.applthermaleng.2007.07.019.
[9] Di Battista D, Di Bartolomeo M, Villante C, Cipollone R. On the limiting factors of the waste heat recovery via ORC-based power units for on-the-road transportation sector. Energy Convers Manag 2018;155:68–77. https://doi.org/10.1016/J.Enconman.2017.10.091.
[10] Desideri A, Hernandez A, Gusev S, van den Broek M, Lemort V, Quoilin S. Steady-state and dynamic validation of a small-scale waste heat recovery system using the ThermoCycle Modelica library. Energy 2016;115:684–96. https://doi.org/10.1016/j.energy.2016.09.004.
[11] Kosmadakis G, Manolakos D, Papadakis G. Experimental investigation of a low-temperature organic Rankine cycle (ORC) engine under variable heat input operating at both subcritical and supercritical conditions. Appl Therm Eng 2016;92:1–7. https://doi.org/10.1016/J.Applthermaleng.2015.09.082.
[12] Quoilin S, Aumann R, Grill A, Schuster A, Lemort V, Spliethoff H. Dynamic modeling and optimal control strategy of waste heat recovery Organic Rankine Cycles. Appl Energy 2011;88:2183–90. https://doi.org/10.1016/j.apenergy.2011.01.015.
[13] Ni J, Zhao L, Zhang Z, Zhang Y, Zhang J, Deng S, et al. Dynamic performance investigation of organic Rankine cycle driven by solar energy under cloudy condition. Energy 2018;147:122–41. https://doi.org/10.1016/J.ENERGY.2018.01.032.
[14] Mazzi N, Rech S, Lazzaretto A. Off-design dynamic model of a real Organic Rankine Cycle system fuelled by exhaust gases from industrial processes. Energy 2015;90:537–51. https://doi.org/10.1016/j.energy.2015.07.083.
[15] Casella F, Mathijssen T, Colonna P, Van J, Tri-O-Gen B. Dynamic modeling of organic rankine cycle power systems. doi:10.1115/1.4023120.
[16] Usman M, Imran M, Lee DH, Park B-S. Experimental investigation of off-grid organic Rankine cycle control system adapting sliding pressure strategy under proportional integral with feed-forward and compensator. Appl Therm Eng 2017;110:1153–63. https://doi.org/10.1016/J.Applthermaleng.2016.09.021.
[17] Padula F, Sandrini R, Cominardi G. Adaptive PI control of an organic Rankine cycle power plant. IFAC Proc 2012;45:459–64. https://doi.org/10.3182/20120328-3-IT-3014.00078.
[18] Hernandez A, Desideri A, Ionescu C, De Keyser R, Lemort V, Quoilin S. Real-time optimization of organic Rankine cycle systems by extremum-seeking control. Energies 2016;9:334. https://doi.org/10.3390/en9050334.
[19] Hernandez A, Desideri A, Gusev S, Ionescu CM, Den Broek M Van, Quoilin S, et al. Design and experimental validation of an adaptive control law to maximize the power generation of a small-scale waste heat recovery system. Appl Energy 2017;203:549–59. https://doi.org/10.1016/J.Apenergy.2017.06.069.
[20] Marchionni M, Bianchi G, Karvountzis-Kontakiotis A, Pesiridis A, Tassou SA. Dynamic modeling and optimization of an ORC unit equipped with plate heat exchangers and turbomachines. Energy Procedia 2017;129:224–31. https://doi.org/10.1016/J.Egypro.2017.09.146.
[21] Gamma T. Gamma technologies inc. GT-SUITE Flow theory manual. 2017.
[22] Lemmon EW, Huber Marcia L, Refprop Mom. NIST standard reference database 23. 2013., Version 9.1.
[23] SSP G7 - SWEP http://swep.net/support/ssp-calculation-software/ssp-g7/.
[24] Cipollone R, Bianchi G, Di Battista D, Fatigati F. Experimental and numerical analyses on a plate heat exchanger with phase change for waste heat recovery at off-design conditions. J Phys Conf Ser 2015;655:12038. https://doi.org/10.1088/1742-6596/655/1/012038.
[25] Prosperetti A. A generalization of the Rayleigh–Plesset equation of bubble dynamics. Phys Fluids 1982;25:409. https://doi.org/10.1063/1.863775.
[26] Yan Y-Y, Lio H-C, Lin T-F. Condensation heat transfer and pressure drop of refrigerant R-134a in a plate heat exchanger. Int J Heat Mass Tran 1999;42:993–1006. https://doi.org/10.1016/S0017-9310(98)00217-8.
[27] Alshammari F, Karvountzis-Kontakiotis A, Pesiridis A, Giannakakis P. Off-design performance prediction of radial turbines operating with ideal and real working fluids. Energy Convers Manag 2018;171:1430–9. https://doi.org/10.1016/J.Enconman.2018.06.093.
[28] Moustapha H, Zelesky M, Baines N, Japikse D. Axial and radial turbines. ConceptsnrecCom. 2003. p. 10.
[29] Aungier R. Preliminary aerodynamic design of axial-flow turbine stages. Turbine aerodyn. Axial-flow radial-flow turbine des. Anal.., Three Park Avenue New York, NY 10016-5990: ASME; n.d., p. 133–166. doi:10.1115/1.802418.ch6.

Nomenclature

β: Blade angle [deg]
ε: Clearance [mm]
ζ: Fanning friction factor
η: Efficiency
ρ: Density [kg/m^3]
μ: Kinematic viscosity [kg/(ms)]
ξ: Pressure loss coefficient
σ: Surface tension [Pa]
υ: Dynamic viscosity [m^2/s]
φ: Flow coefficient
ψ: Loading coefficient
c: Axial velocity [m/s]
dx: Displacement [m]
h: Heat transfer coefficient [W/(m^{2}K)]
k: Thermal conductivity [W/(mK)]
m'': Mass flux [kg/(m^{2}s)]
$\dot{m}$: Mass flow rate [kg/s]
p: Pressure [bar]
q'': Heat flux [W/m^2]
t: Time [s]
u: Peripheral speed [m/s]
v: Absolute velocity [m/s]
w: Relative velocity [m/s]
x: Quality
A: Area [m^2]
D: Diameter [m]
H: Specific enthalpy [kJ/kg]
K: Discharge coefficient
L: Length [m]
Ma: Mach number
Nu: Nusselt number
Pr: Prandtl number
R, r: Radius [m]
Re: Reynolds number
T: Temperature [K]
W: Specific work [J]
$\dot{W}$: Power [W]
Z: Number of blades

subscripts

θ: tangential
b: bubble, back face
$bound$: boundaries
c: curvature
e: electric
eq: equivalent
h: hub
hyd: hydraulic
inc: incidence
is: isentropic
l: liquid

m: meridional
o: outlet
opt: optimized
pass: passage
r: radial
real: real
rot: rotor
st: stator
t: ,*tip* blade tip
th: thermal
ts: total to static
v: vapour
wl: wall
wf: working fluid
x: axial
∞*:* infinite
0*:* total

Acronyms

OP: Only Pump
OT: Only Turbine
ORC: Organic Rankine Cycle
PI: Proportional-Integral
PT: Pump and Turbine
PV: Pump and Valve
TIT: Turbine Inlet Temperature
WHR: Waste Heat Recovery